


Cite this: *RSC Adv.*, 2018, 8, 36596

# Versatility of CoPcS in CoPcS/TiO<sub>2</sub> for MB degradation: photosensitization, charge separation and oxygen activation

Zhao Gao,  Hanpei Yang,\* Hongyu Zhu, Runqiang Guo and Junmin Wu

In this report, a composite photocatalyst consisting of cobalt phthalocyanine sulfate (CoPcS) and TiO<sub>2</sub> was prepared by a facile synthesis. Careful characterizations and measurements indicate a covalent grafting of CoPcS onto TiO<sub>2</sub> through Ti–O–S linkages, acquiring an intimate heterojunction between TiO<sub>2</sub> and CoPcS. The obtained composite was evaluated for its photocatalytic activity toward the degradation of methyl blue (MB) under visible light irradiation. The evaluation showed a significantly enhanced degradation rate of MB by CoPcS/TiO<sub>2</sub>. The improved photocatalytic performance of CoPcS/TiO<sub>2</sub> was attributed to the photosensitization of TiO<sub>2</sub> by CoPcS, charge separation by electron transfer at the interface of the heterojunction formed between CoPcS and TiO<sub>2</sub>, and oxygen activation *via* CoPcS. A synergetic mechanism in improving the photocatalytic performance of TiO<sub>2</sub> by CoPcS was investigated.

Received 23rd July 2018  
Accepted 18th October 2018

DOI: 10.1039/c8ra06161k

rsc.li/rsc-advances

## 1. Introduction

Over the past few decades, titanium dioxide (TiO<sub>2</sub>) has been widely studied in pollution control.<sup>1</sup> However, it usually shows inertness under visible light irradiation and low quantum yield in light energy utilization.<sup>2</sup> Recent strategies focused on grafting photosensitizers or semiconductors onto TiO<sub>2</sub> for expanding their ranges of light absorbance and inhibiting the recombination of photogenerated electron–hole pairs.<sup>3,4</sup>

For an effective photosensitizer of TiO<sub>2</sub>, two important criteria are required:<sup>5</sup> the photoactive compound should have a high extinction coefficient in the visible region, and be capable of being adsorbed on the TiO<sub>2</sub> surface *via* physical/chemical interaction. In constructing heterojunctions, the band gap of the semiconductor used to modify TiO<sub>2</sub> should be narrow, and its conduction and valence band positions should be matched with that of TiO<sub>2</sub>, respectively.<sup>4</sup> On these accounts, metal phthalocyanines (MPcs, M = Fe, Co) are benign candidates for the modification of TiO<sub>2</sub>. More interestingly, the M–N<sub>4</sub> structure in MPcs can increase the O–O length of oxygen, which would play an important role in promoting the production of superoxide radical ( $\cdot\text{O}_2^-$ ) from O<sub>2</sub>.<sup>6</sup> Many efforts have been devoted to coupling of MPcs with TiO<sub>2</sub>.<sup>3,7,8</sup> However, the recognition on the versatility of MPcs in photocatalysis is insufficient, especially, the function of MPcs in activating oxygen in the process of degrading organic pollutants.

In this report, cobalt phthalocyanine sulfate (CoPcS) was composited with TiO<sub>2</sub>, and the experiments on MB degradation

over CoPcS/TiO<sub>2</sub> were conducted. The multiple roles of CoPcS in composite were investigated and synergy in photosensitization, charge separation and oxygen activation was proposed.

## 2. Experimental

### 2.1. Synthesis of samples

All the reagents used in this experiment were received without further purification. The CoPcS/TiO<sub>2</sub> composite was fabricated *via* a hydrothermal route. In a typical preparation, 60 mg CoPcS (optical) and 20 ml absolute ethyl alcohol were mixed and ultrasounded for 30 min to get a homogeneous turbid liquid. Subsequently, another 16 ml absolute ethyl alcohol, 3.2 ml acetic acid and 10 ml Ti(C<sub>4</sub>H<sub>9</sub>O)<sub>4</sub> were added into the mixture, followed by dropwise addition of 2 ml deionized water under vigorous stirring for 1 h. Then, the compound was loaded into a 100 ml stainless steel autoclave, sealed and moved into an oven and kept at 180 °C for 10 h. After cooling the autoclave to room temperature, the precipitate was washed with ethanol and deionized water thrice, and then dried at 80 °C for 24 h. Finally, the solid was annealed at 300 °C for 2 h in purity N<sub>2</sub>. For comparison, TiO<sub>2</sub> were prepared under same procedure without adding of CoPcS.

### 2.2. Characterizations and measurements

X-ray diffraction (XRD) analysis were performed on a Shimadzu-3A diffractometer at 40 kV and 30 mA with Cu K $\alpha$  radiation ( $\lambda$  = 0.15418 nm). The morphologies were examined by transmission electron microscopy (TEM, JEM-2100CX, JEOL). Infrared spectra (FT-IR) were acquired with an 8400S spectrometer (Shimadzu) in the transmission mode. X-ray photoelectron spectra (XPS)

Key Laboratory of Integrated Regulation and Resource Development on Shallow Lakes, Ministry of Education, College of Environment, Hohai University, Nanjing 210098, China. E-mail: yanghanpei@hhu.edu.cn; Fax: +86 25 83786090; Tel: +86 25 84968465



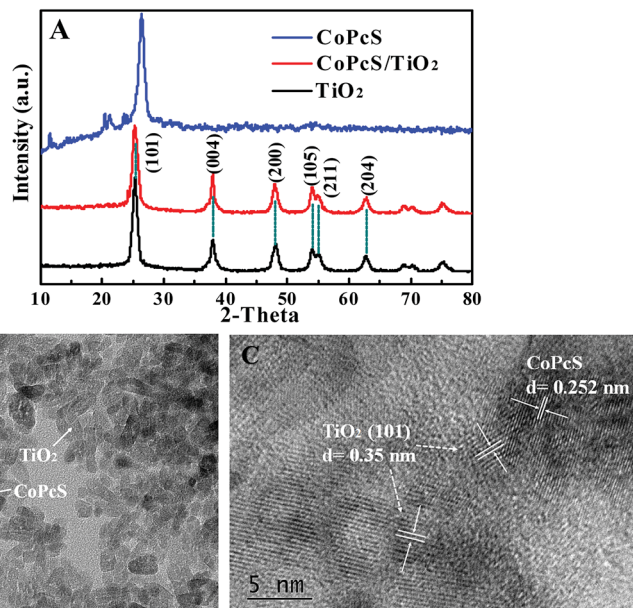


Fig. 1 XRD patterns of samples (A), TEM (B) (inset is that of pure  $\text{TiO}_2$ ) and HRTEM (C) image of  $\text{CoPcS}/\text{TiO}_2$ .

were obtained by a PHI 5000 Versa Probe spectrometer (ULVAC-PHI) operated at a voltage of 13 kV and an emission current of 28 mA using Al K $\alpha$  as exciting source (1486.6 eV). The binding energies were referenced to C 1s at 284.5 eV. The UV-vis absorption spectra of samples were obtained from a Shimadzu UV-3600 spectrophotometer equipped with an integrating sphere using  $\text{BaSO}_4$  as reference. Photoluminescence (PL) spectra were recorded on F-7000 fluorescence spectrophotometer (Hitachi) with a laser excitation of 420 nm. Electron paramagnetic resonance (EPR) signals of paramagnetic species spin-trapped with DMPO were recorded at ambient temperature (298 K) with a Bruker EPR 300E spectrometer, the irradiation source ( $\lambda = 532$  nm) was a Quanta-Ray Nd:YAG (10 pluses per second) laser system.

### 2.3. Photocatalytic oxidation experiments

The visible-light-driven photocatalytic activity of the as-prepared samples was monitored from the results of the degradation of MB. For each photocatalytic activity measurements, 10 mg of as-prepared catalysts were dispersed into 100 ml of MB solution initialized at  $5 \text{ mg L}^{-1}$ . The light comes from a 300 W xenon lamp (CEL-HXF-300, Education Au-light Co., Ltd., Beijing, China) equipped with a UV cutoff filter ( $\lambda \geq 400$  nm). The photocatalytic reactions took place in the reactor connected to a water bath to main the solution at about  $25^\circ\text{C}$  and the reaction aqueous slurries were magnetic stirred and bubbled with air at a flow rate of  $40 \text{ ml min}^{-1}$ . The suspension was stirred in the dark for 1 h to obtain adsorption equilibrium of MB before illumination. During the photo-reaction, samples were collected at selected time intervals. The catalyst powders were removed by filtration and the residual concentration of MB was determined by the spectrophotometer. Quenching experiments were conducted under same conditions except the existence of each scavenger in 10 mM of ethylenediamine

tetraacetic acid disodium ( $\text{EDTA-Na}_2$ , for  $\cdot\text{O}_2^-$ ), *tert*-butyl alcohol (*t*BA, for  $\cdot\text{OH}$ ) and *p*-benzoquinone (pBQ, for  $\text{h}^+$ ).

## 3. Results and discussion

### 3.1. Morphology and structure

**3.1.1. XRD and TEM analysis.** Fig. 1A shows the XRD patterns of the as-prepared samples. The spectrum of bare  $\text{TiO}_2$  and  $\text{CoPcS}/\text{TiO}_2$  show the typical peaks of anatase phase (JCPDS no. 21-1272), while the diffraction peaks of  $\text{CoPcS}$  were not observed on the XRD pattern of  $\text{CoPcS}/\text{TiO}_2$  probably due to the low loading mass or small size of loaded  $\text{CoPcS}$ .<sup>9</sup> The average crystallite sizes of pure  $\text{TiO}_2$  and  $\text{CoPcS}/\text{TiO}_2$  were calculated to be 9.9 and 9.2 nm, respectively, based on the Scherrer formula. TEM observations of  $\text{CoPcS}/\text{TiO}_2$  (Fig. 1B) indicate an intimate coating of  $\text{CoPcS}$  on  $\text{TiO}_2$ , and particle sizes roughly matched to that from XRD. As shown in Fig. 1C, the HRTEM image of  $\text{CoPcS}/\text{TiO}_2$  displays two types of clear lattice fringes, one set of the fringe spacing ( $d$ ) was *ca.* 0.35 nm, corresponding to the (101) plane of the anatase crystal structure of  $\text{TiO}_2$ ,<sup>10</sup> another set of stacking feature ( $d \approx 0.252$  nm) corresponds to the  $\text{CoPcS}$ .<sup>11</sup> The result agrees well with that from the XRD analysis.

**3.1.2. FTIR analysis.** The surface structures of resultant samples were revealed by FT-IR spectra as shown in Fig. 2A. The spectrum of pure  $\text{TiO}_2$  shows the Ti–O–Ti at  $539 \text{ cm}^{-1}$ , Ti–O–H at  $1654$  and  $3468 \text{ cm}^{-1}$ .<sup>12,13</sup> The spectrum recorded on  $\text{CoPcS}/\text{TiO}_2$  shows distinct difference from what on pure  $\text{TiO}_2$  with C–C at  $1404$ ,<sup>14</sup> C=C and C=N at  $1638 \text{ cm}^{-1}$ .<sup>15,16</sup> The peak centered at  $917$ ,  $1040$  and  $1232 \text{ cm}^{-1}$  is attributed to Co–N,<sup>17</sup> C–N<sup>14</sup> and S–O<sup>18</sup> in  $\text{CoPcS}$ , sequentially. The broad peak at  $608 \text{ cm}^{-1}$  is induced by Ti–O–Ti and Ti–O–S. This is a strong evidence of covalent attaching of  $\text{CoPcS}$  on  $\text{TiO}_2$ . The linkage between  $\text{CoPcS}$  and  $\text{TiO}_2$  is proposed as Fig. 2B.

**3.1.3. XPS analysis.** The surface structure of  $\text{CoPcS}/\text{TiO}_2$  was confirmed by XPS. In Fig. 3A, the peaks of C 1s in  $\text{CoPcS}/$



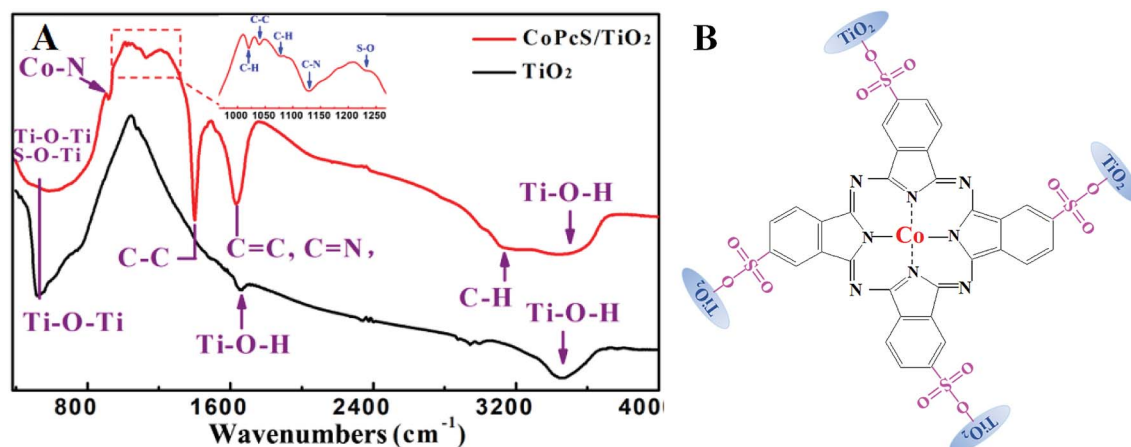


Fig. 2 FT-IR spectra on  $\text{TiO}_2$  and  $\text{CoPcS}/\text{TiO}_2$  (A) and the possible linkage between  $\text{CoPcS}$  and  $\text{TiO}_2$  (B).

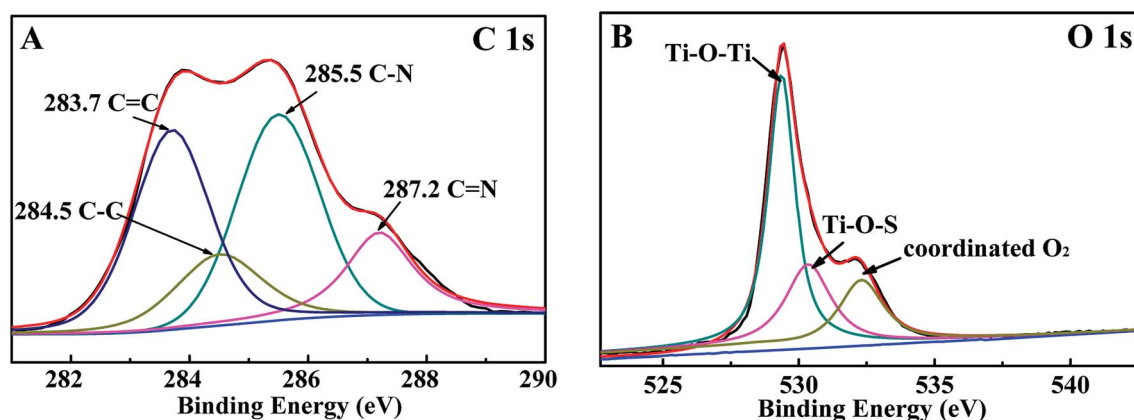


Fig. 3 High-resolution XPS spectra of C 1s (A) and O 1s (B) in  $\text{CoPcS}/\text{TiO}_2$ .

$\text{TiO}_2$  can be deconvoluted into four lines peaked at 283.7, 284.5, 285.5 and 287.2 eV, corresponding to  $\text{C}=\text{C}$ ,  $\text{C}-\text{C}$ ,  $\text{C}-\text{N}$  and  $\text{C}=\text{N}$  in  $\text{CoPcS}$ , respectively.<sup>19–22</sup> The O 1s (Fig. 3B) composed of three peaks, the deconvoluted peak observed at 529.3 eV corresponds to the  $\text{Ti}-\text{O}-\text{Ti}$  in  $\text{TiO}_2$ . The peak at a binding energy of 530.4 eV is attributed to  $\text{Ti}-\text{O}-\text{S}$ ,<sup>23</sup> indicating a covalent linkage between  $\text{CoPcS}$  and  $\text{TiO}_2$ . An obvious component with the binding energy at 532.4 eV can be assigned to the oxygen ( $\text{*O}_2$ ) coordinated by  $\text{CoPcS}$ .<sup>24</sup>

### 3.2. Photocatalytic activity of samples

As shown in Fig. 4A, the removal of MB by direct photolysis or photocatalytic degradation on  $\text{CoPcS}$  was observed negligible. Pure  $\text{TiO}_2$  exhibited nearly 28.3% of MB degradation mainly attributed to their visible-light-driven activity under self-photosensitization of MB.<sup>25</sup> The  $\text{CoPcS}/\text{TiO}_2$  exhibited superior performance on the MB degradation, with the degradation rate of 88% and the pseudo-first-order rate constant of  $0.0091 \text{ min}^{-1}$  (almost 6.2 times of that on pure  $\text{TiO}_2$ ). Remarkably, obvious decrease in MB degradation was observed on  $\text{CoPcS}/\text{TiO}_2$  under anaerobic conditions (by bubbling  $\text{N}_2$ ), suggesting that  $\text{O}_2$  was crucial in the reaction.

### 3.3. Versatility of $\text{CoPcS}$ in $\text{CoPcS}/\text{TiO}_2$ for MB degradation

**3.3.1. Photosensitization.** As depicted in Fig. 5A, the absorption spectrum recorded on  $\text{TiO}_2$  exhibited a typical behavior of a wide-band-gap oxide semiconductor, with no absorption in visible region. However, the  $\text{CoPcS}/\text{TiO}_2$  exhibited strong absorption of light in whole wavelength region. Moreover, the spectrum showed an obvious red-shift of absorption edge to approximately 445 nm, and typical peaks of Q band from dimer and monomer  $\text{CoPcS}$  at 603 and 669  $\text{nm}^{-1}$ <sup>17</sup> resulted from the excitation from their HOMO to the LUMO.<sup>26,27</sup> Compared to the regular  $\text{CoPcS}$ , the peaks in Q band of  $\text{CoPcS}/\text{TiO}_2$  exhibited red and blue shifts slightly, suggesting the electronic coupling between  $\text{CoPcS}$  and  $\text{TiO}_2$  due to the  $\text{Ti}-\text{O}-\text{S}$  linkage indicated by IR and XPS.<sup>28,29</sup> The energy band gaps from the UV-vis DRS spectra were deduced from the Tauc plot using the Kubelka-Munk theory, and the result was shown as Fig. 5B. The band gap energy of  $\text{TiO}_2$  was determined as  $\sim 3.2 \text{ eV}$ , while that of  $\text{CoPcS}/\text{TiO}_2$  was calculated to be  $\sim 2.7 \text{ eV}$ , which matched well with the absorption edge at 445 nm.

Under visible light irradiation of  $\text{CoPcS}/\text{TiO}_2$ , the singlet excited state ( $\text{S}_1$ ) of  $\text{CoPcS}$  would typically generated from the ground state ( $\text{S}_0$ ) and then transformed to triplet excited state



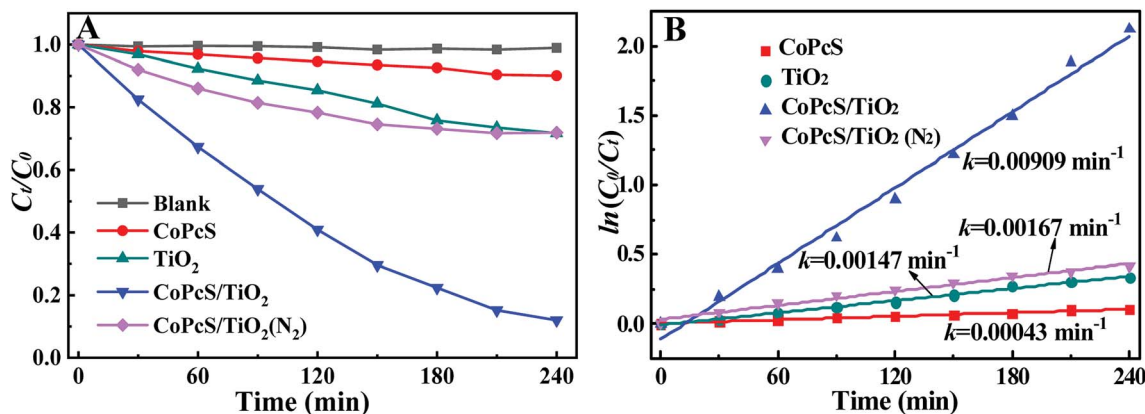


Fig. 4 Photocatalytic degradation of MB on samples (A) and pseudo-first order fitting of the photocatalytic data (B), ( $C_0$  in (A) and B) represent the actual concentrations of MB after their adsorption-desorption equilibrium in the dark.

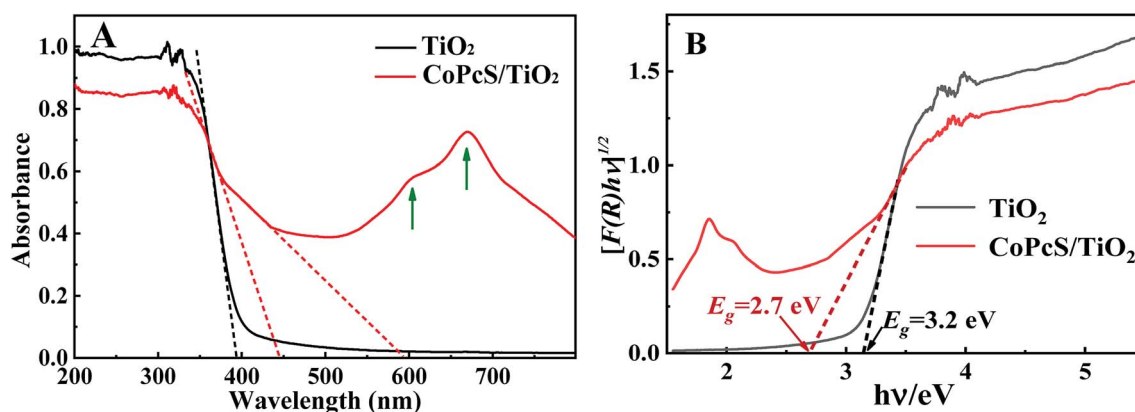


Fig. 5 UV-vis diffuse reflectance absorption spectra (A) and their Tauc plot (B) of  $\text{TiO}_2$  and  $\text{CoPcS}/\text{TiO}_2$ .

( $T_1$ ) through intersystem crossing.<sup>30</sup> The redox potential of  $S_0$ ,  $S_1$  and  $T_1$  of CoPcS are around 0.46,  $-1.35$  and  $-0.75 \text{ eV}$  (vs. NHE), respectively.<sup>31,32</sup> The generation of  $S_1$  is normally negligible due to their short lifetime (ns),<sup>33</sup> but the excited CoPcS in  $T_1$  (ms) can inject charges into the conduction band of  $\text{TiO}_2$ , generating cation radicals of CoPcS ( $\text{CoPcS}^{+\bullet}$ ). The  $\text{CoPcS}^{+\bullet}$  can participate directly in the degradation of MB<sup>33</sup> and contributes

to the enhanced activity of  $\text{CoPcS}/\text{TiO}_2$  showed by Fig. 4. Herein, the photosensitization of  $\text{TiO}_2$  by CoPcS can be expressed as follows:

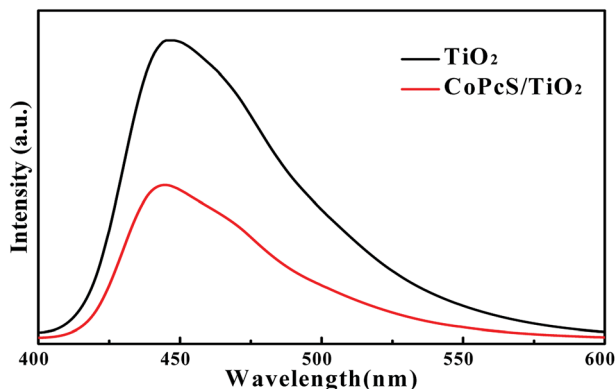
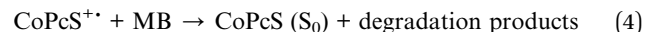


Fig. 6 PL spectra of  $\text{TiO}_2$  and  $\text{CoPcS}/\text{TiO}_2$ .

**3.3.2. Charge separation.** It is well accepted that CoPcS is a typical narrow-band-gap semiconductor with its  $E_g$  of about  $2.1 \text{ eV}$ .<sup>34</sup> Coupling  $\text{TiO}_2$  with CoPcS also contributed to the absorption of visible light on  $\text{CoPcS}/\text{TiO}_2$ . As indicated in Fig. 5, the  $\text{CoPcS}/\text{TiO}_2$  showed significant light adsorption in 445–595 nm, which was consistent with the band gap of CoPcS. In addition, the formed heterojunction between CoPcS and  $\text{TiO}_2$  played an important role in the separation of photogenerated electron-hole pairs. The conduction band edges of  $\text{TiO}_2$  and CoPcS are  $-0.5$  and  $-1.05 \text{ eV}$ , respectively.<sup>35–38</sup> The





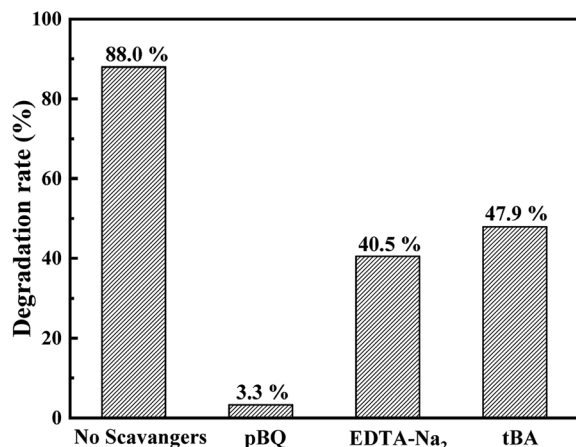


Fig. 7 Degradation rates of MB over CoPcS/TiO<sub>2</sub> in solutions with and without scavengers.

photogenerated electrons were able to transfer from the conduction band of CoPcS to that of TiO<sub>2</sub>, leaving holes on the valence band of CoPcS. In this way, the photogenerated electron-hole pairs on CoPcS got separated.

Charge separation on the heterojunction was confirmed by PL measurement. As demonstrated by Fig. 6, the remarkable decrease in PL intensity demonstrated that deposition of CoPcS onto TiO<sub>2</sub> decreased the carrier recombination rate and improves the separation efficiency of photogenerated electrons and holes, which was favorable to the degradation of MB.<sup>39</sup>

**3.3.3. Oxygen activation.** As identified by the quenching experiments illustrated in Fig. 7,  $\cdot\text{O}_2^-$ ,  $\cdot\text{OH}$  and  $\text{h}^+$  all played significant roles in proceeding MB degradation, especially the  $\cdot\text{O}_2^-$ , which is generated predominantly through the trapping of photo-excited electrons by dissolved molecular oxygen. For the redox potential of holes on the valence band of CoPcS is negative than E ( $\text{H}_2\text{O}/\cdot\text{OH}$ ), we deduce that  $\cdot\text{OH}$  is generated from  $\cdot\text{O}_2^-$ .<sup>40</sup>

The presence of  $\cdot\text{O}_2^-$  and  $\cdot\text{OH}$  radicals was further confirmed by the electron spin response (ESR) experiments of CoPcS/TiO<sub>2</sub> with 5,5-dimethyl-1-pyrroline (DMPO) as a scavenger in a methanol and an aqueous solution. The four

characteristic peaks of DMPO- $\cdot\text{O}_2^-$ <sup>41</sup> (Fig. 8A) and the system signature (1 : 2 : 2 : 1 signals) of DMPO- $\cdot\text{OH}$  radical adducts<sup>42</sup> (Fig. 8B) were both observed. In contrast, no DMPO- $\cdot\text{O}_2^-$  and DMPO- $\cdot\text{OH}$  signals emerged for bare TiO<sub>2</sub> dispersion.

According to the above results, we consider that oxygen in the reaction is activated by the Co-N<sub>4</sub> structure in CoPcS. The electronic configuration of 3d orbital of free Co<sup>2+</sup> (in spherical field) is diagrammatically presented as Fig. 10 (a). In a square-planar crystal field offered by CoPcS in Fig. 2B, the degenerate energy level of 3d-orbitals split into four levels as sketched as (b).<sup>43</sup> Coordination of dioxygen (as a fifth ligand<sup>44</sup>) to Co<sup>2+</sup> surrounded by the macrocyclic ligand as CoPcS cause a further rearranging of energy into two levels with e<sub>g</sub> and t<sub>2g</sub> symmetry as (c) in Fig. 9.<sup>45</sup> However, this octahedral symmetric configuration in a non-linear molecular is instable due to the non-full occupation in 3d orbital of Co<sup>2+</sup>,<sup>46</sup> the configuration will be distorted as (d) by a Jahn-Teller effect.<sup>47</sup>

In such a configuration, most of the interpretations of experimental and theoretical investigation coincided in the conclusion that the 3d<sub>z<sup>2</sup></sub> orbital is half filled.<sup>48</sup> A  $\sigma$ -rich orbital of O<sub>2</sub> donates electron density to 3d<sub>z<sup>2</sup></sub> of Co<sup>2+</sup>, forming a  $\sigma$ -type bond, while a  $\pi$  interaction is produced between the d <sub>$\pi$</sub>  (d<sub>xz</sub>, d<sub>yz</sub>) orbitals and  $\pi^*$  orbitals of dioxygen, with charge transfer from metal to O<sub>2</sub>.<sup>49</sup> This electrons rearranging get oxygen activated and increase the O-O bond length from the usual 1.21 to ~1.30 Å.<sup>6</sup> According to literature, the redox potential of oxygen in ground state E ( $^3\text{O}_2/\cdot\text{O}_2^-$ ) is around -0.048 eV.<sup>50</sup> However, with the activation, the potential value can increase to ~0.77 eV,<sup>6</sup> which is more positive than that of E<sub>CB</sub> in TiO<sub>2</sub>.

Based on the above results, the synergy of photosensitization, charge separation and oxygen activation on CoPcS/TiO<sub>2</sub> was proposed as Fig. 10. The electrons generated by photosensitization and charge separation on the conduction band of TiO<sub>2</sub> can be more easily trapped by the activated oxygen ( $^*\text{O}_2$ ), deriving more  $\cdot\text{O}_2^-$  species participating in degrading MB. Some of the  $\cdot\text{O}_2^-$  reacts with H<sup>+</sup>, followed by producing  $\cdot\text{OH}$  of a redox potential of 2.4 eV. The redox potentials of generated CoPcS<sup>+</sup> and holes were 1.2 and 1.05 eV, respectively.<sup>37,38</sup> Thus, the MB was oxidized by  $\cdot\text{OH}$ , CoPcS<sup>+</sup> and holes. By this way, the photocatalytic activity of CoPcS/TiO<sub>2</sub> in degrading MB was enhanced.

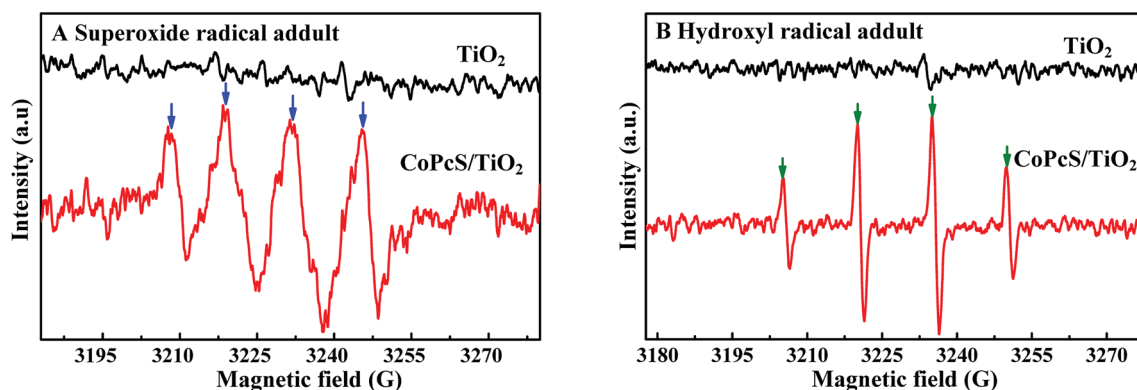


Fig. 8 DMPO spin-trapping ESR spectra recorded with as-prepared samples in (A) methanol dispersion (for DMPO- $\cdot\text{O}_2^-$ ) and (B) aqueous dispersion (for DMPO- $\cdot\text{OH}$ ) under visible light irradiation.



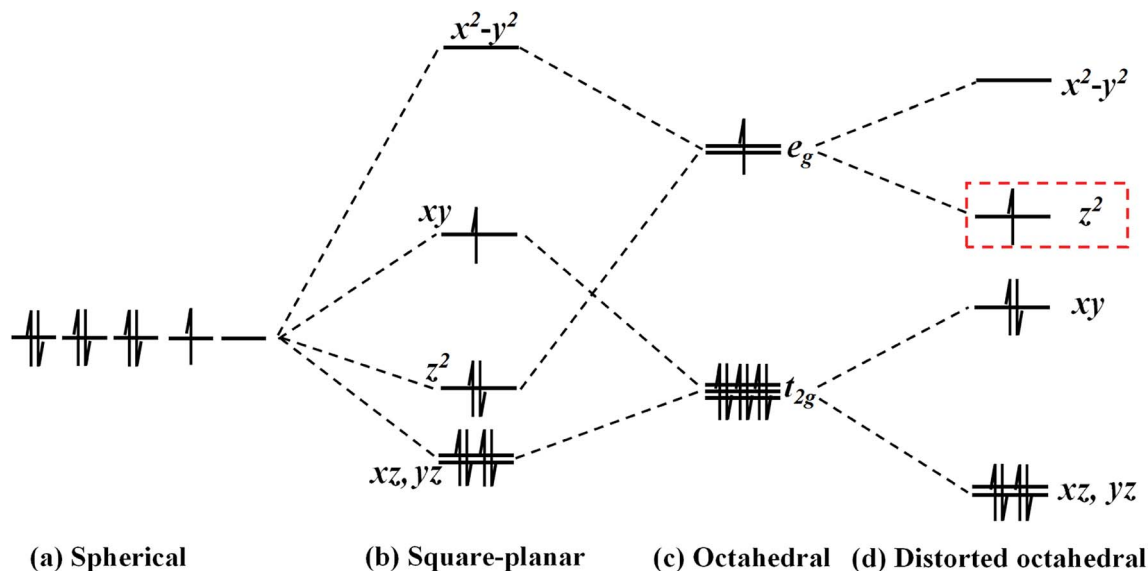


Fig. 9 Sketch of the energy splitting of  $\text{Co}^{2+}$  in different crystal field.

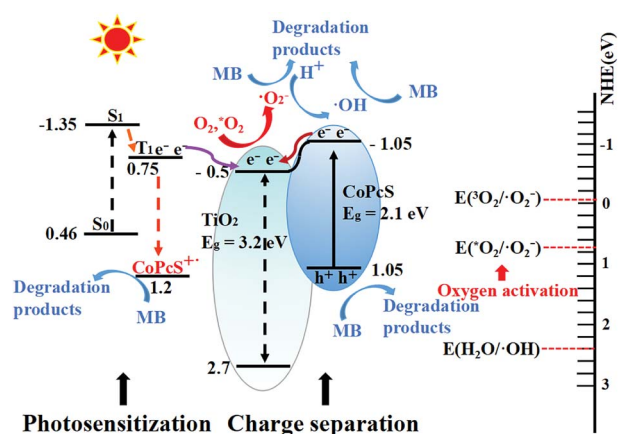


Fig. 10 A schematic diagram of the synergetic mechanism in MB degradation on CoPcS/TiO<sub>2</sub>.

## 4. Conclusion

In this work, TiO<sub>2</sub> was composited with CoPcS *via* the Ti–O–S linkage. The photosensitization of TiO<sub>2</sub> by CoPcS and charge separation on the heterojunction were promoted. At the same time, the oxygen was activated by CoPcS. Due to the versatility of CoPcS on TiO<sub>2</sub>, the degradation rate of MB over CoPcS/TiO<sub>2</sub> reached 88% under visible light in 4 h. This synergy is of great potential for design of high-photoreactive catalysts using CoPcS as a component.

## Conflicts of interest

There are no conflicts to declare.

## Acknowledgements

The project was financially supported by the Foundation of National Key Scientific Instrument and Equipment Development Project of China (No. 2014YQ060773), the Priority Academic Program Development of Jiangsu Higher Education Institutions.

## References

- 1 G. Y. Rao, Q. Y. Zhang, H. L. Zhao, J. T. Chen and Y. Li, Novel titanium dioxide/iron (III) oxide/graphene oxide photocatalytic membrane for enhanced humic acid removal from water, *Chem. Eng. J.*, 2016, **302**, 633–640.
- 2 I. C. Kang, Q. Zhang, S. Yin, T. Sato and F. Saito, Improvement in photocatalytic activity of TiO<sub>2</sub> under visible irradiation through addition of N-TiO<sub>2</sub>, *Environ. Sci. Technol.*, 2008, **42**(10), 3622–3626.
- 3 Q. Sun and Y. M. Xu, Sensitization of TiO<sub>2</sub> with aluminum phthalocyanine: factors influencing the efficiency for chlorophenol degradation in water under visible light, *J. Phys. Chem. C*, 2009, **113**, 12387–12394.
- 4 Q. C. Xu, D. V. Wellia, Y. H. Ng, R. Amal and T. T. Y. Tan, Synthesis of porous and visible-light absorbing Bi<sub>2</sub>WO<sub>6</sub>/TiO<sub>2</sub> heterojunction films with improved photoelectrochemical and photocatalytic performances, *J. Phys. Chem. C*, 2011, **115**, 7419–7428.
- 5 P. V. Kamat, Photoelectrochemistry in particulate systems. 9. Photosensitized reduction in a colloidal titania system using anthracene-9-carboxylate as the sensitizer, *J. Phys. Chem.*, 1989, **93**, 859–864.
- 6 S. Kattel, P. Atanassov and B. Kiefer, Catalytic activity of Co-N<sub>x</sub>/C electrocatalysts for oxygen reduction reaction: a density functional theory study, *Phys. Chem. Chem. Phys.*, 2013, **15**, 148–153.



- 7 Z. C. Guo, B. Chen, J. B. Mu and M. Y. Zhang, Iron phthalocyanine/TiO<sub>2</sub> nanofiber heterostructures with enhanced visible photocatalytic activity assisted with H<sub>2</sub>O<sub>2</sub>, *J. Hazard. Mater.*, 2012, **219–220**, 156–163.
- 8 A. Ebrahimi, M. A. Zanjanchi, H. Noei, M. Arvand and Y. Wang, TiO<sub>2</sub> nanoparticles containing sulphonated cobalt phthalocyanine: Preparation, characterization and photocatalytic performance, *J. Environ. Chem. Eng.*, 2014, **2**, 484–494.
- 9 K. Wang, J. J. Xu and K. S. Tang, Solid-contact potentiometric sensor for ascorbic acid based on cobalt phthalocyanine nanoparticles as ionophore, *Talanta*, 2005, **67**, 798–805.
- 10 Z. C. Guo, B. Chen, J. B. Mu and M. Y. Zhang, Iron phthalocyanine/TiO<sub>2</sub> nanofiber heterostructures with enhanced visible photocatalytic activity assisted with H<sub>2</sub>O<sub>2</sub>, *J. Hazard. Mater.*, 2012, **219–220**, 156–163.
- 11 B. Z. Zhao, X. D. Niu, X. R. Hao, Y. Y. Li, Q. Fu and Y. G. Chen, Research in the energy band structures for transition metalphthalocyanine compounds, *J. Northeast Norm. Univ.*, 2004, **36**(3), 66–69.
- 12 S. Yurdakul and S. Badoğlu, FT-IR spectra, vibrational assignments, and density functional calculations of imidazo[1,2-a]pyridine molecule and its Zn(II) halide complexes, *Struct. Chem.*, 2009, **20**(3), 423–434.
- 13 S. X. Liu, X. Y. Chen and X. A. Chen, TiO<sub>2</sub>/AC composite photocatalyst with high activity and easy separation prepared by a hydrothermal method, *J. Hazard. Mater.*, 2007, **143**(1), 257–263.
- 14 R. Seoudi, G. S. El-Bahy and Z. A. E. Sayed, FTIR, TGA and DC electrical conductivity studies of phthalocyanine and its complexes, *J. Mol. Struct.*, 2005, **753**, 119–126.
- 15 T. C. Canevari, J. Arguello, M. S. P. Franciso and Y. Gushikem, Cobalt phthalocyanine prepared in situ on a sol-gel derived SiO<sub>2</sub>/SnO<sub>2</sub> mixed oxide: Application in electrocatalytic oxidation of oxalic acid, *J. Electroanal. Chem.*, 2007, **609**(2), 61–67.
- 16 N. Sundaraganesan, S. Kalaichelvan, C. Meganathan, B. D. Joshua and J. Cornard, FT-IR, FT-Raman spectra and ab initio HF and DFT calculations of 4-N,N'-dimethylamino pyridine, *Spectrochim. Acta, Part A*, 2008, **71**(3), 898–906.
- 17 Z. Xu, H. Li, G. Cao, Q. L. Zhang, K. Z. Li and X. N. Zhao, Electrochemical performance of carbon nanotube-supported cobalt phthalocyanine and its nitrogen-rich derivatives for oxygen reduction, *J. Mol. Catal. A: Chem.*, 2011, **335**(1), 89–96.
- 18 L. I. Nan, S. S. Dong, L. V. Wangyang, S. Q. Huang, H. X. Chen, Y. Y. Yao and W. X. Chen, Enhanced electrocatalytic oxidation of dyes in aqueous solution using cobalt phthalocyanine modified activated carbon fiber anode, *Sci. China: Chem.*, 2013, **56**(12), 1757–1764.
- 19 M. H. Baek, W. C. Jung, J. W. Yoon, J. S. Hong, Y. S. Lee and J. K. Suh, Preparation, characterization and photocatalytic activity evaluation of micro- and mesoporous TiO<sub>2</sub>/spherical activated carbon, *J. Ind. Eng. Chem.*, 2013, **19**, 469–477.
- 20 M. S. Nahar, J. Zhang, K. Hasegawa, S. Kagaya and S. Kuroda, Phase transformation of anatase–rutile crystals in doped and undoped TiO<sub>2</sub> particles obtained by the oxidation of polycrystalline sulfide, *Mater. Sci. Semicond. Process.*, 2009, **12**, 168–174.
- 21 B. Qiu, Y. Zhou, Y. F. Ma, X. L. Yang, W. Q. Sheng, M. Y. Xing and J. L. Zhang, Facile synthesis of the Ti<sup>3+</sup> self-doped TiO<sub>2</sub>-graphene nanosheet composites with enhanced photocatalysis, *Sci. Rep.*, 2015, **5**, 8591.
- 22 M. Y. Xing, F. Shen, B. Qiu and J. L. Zhang, Highly-dispersed boron-doped graphene nanosheets loaded with TiO<sub>2</sub> nanoparticles for enhancing CO<sub>2</sub> photoreduction, *Sci. Rep.*, 2014, **5**, 6341.
- 23 K. J. Antony Raj, R. Shanmugam, R. mahalakshmi and B. Viswanathan, XPS and IR spectral studies on the structure of phosphate and sulphate modified titania-A combined DFT and experimental study, *Indian J. Chem.*, 2010, **49**, 9–17.
- 24 J. Liu, J. Meeprasert, S. Namuangruk, K. Zha, H. R. Li, L. Huang, P. Maitarad, L. Y. Shi and D. S. Zhang, Facet-activity relationship of TiO<sub>2</sub> in Fe<sub>2</sub>O<sub>3</sub>/TiO<sub>2</sub> nanocatalysts for selective catalytic reduction of NO with NH<sub>3</sub>: in situ DRIFTS and DFT studies, *J. Phys. Chem. C*, 2017, **121**, 4970–4979.
- 25 A. Hosseinnia, M. Keyanpour-Rad and M. Pazouki, Photocatalytic Degradation of Organic Dyes with Different Chromophores by Synthesized Nanosize TiO<sub>2</sub> Particles, *World Appl. Sci. J.*, 2010, **8**, 1327–1332.
- 26 Z. Xu, G. Zhang, Z. Cao, J. S. Zhao and H. J. Li, Effect of N atoms in the backbone of metal phthalocyanine derivatives on their catalytic activity to lithium battery, *J. Mol. Catal. A: Chem.*, 2010, **318**, 101–105.
- 27 L. Edwards and M. Gouterman, Porphyrins: XV. Vapor absorption spectra and stability: phthalocyanines, *J. Mol. Spectrosc.*, 1970, **33**(2), 292–310.
- 28 Z. H. Zhao, J. M. Fan, M. M. Xie and Z. Z. Wang, Photocatalytic reduction of carbon dioxide with in situ synthesized CoPc/TiO<sub>2</sub> under visible light irradiation, *J. Cleaner Prod.*, 2009, **17**(11), 1025–1029.
- 29 T. Ma, K. Inoue, H. Noma, K. Yao and E. Abe, Effect of functional group on photochemical properties and photosensitization of TiO<sub>2</sub>, electrode sensitized by porphyrin derivatives, *J. Photochem. Photobiol., A*, 2002, **152**, 207–212.
- 30 R. Bonnett, Photosensitizers of the porphyrin and phthalocyanine series for photodynamic therapy, *Chem.*, 1995, **26**, 19–33.
- 31 T. Ohno and S. Kato, Electron-transfer reactions of excited phthalocyanines: spin restriction on reaction rate of electron transfer and energy transfer to cobalt compounds, *J. Phys. Chem.*, 2002, **88**, 1670–1674.
- 32 V. Iliev, Phthalocyanine-modified titania—catalyst for photooxidation of phenols by irradiation with visible light, *J. Photochem. Photobiol., A*, 2002, **151**(1), 195–199.
- 33 C. E. Diaz-Urbe, M. C. Daza and F. Maetinez, Visible light superoxide radical anion generation by tetra(4-



- carboxyphenyl)porphyrin/TiO<sub>2</sub>: EPR characterization, *J. Photochem. Photobiol., A*, 2010, **215**, 172–178.
- 34 Z. H. Zhao, J. M. Fan, M. M. Xie and Z. Z. Wang, Photocatalytic reduction of carbon dioxide with in situ synthesized CoPc/TiO<sub>2</sub> under visible light irradiation, *J. Cleaner Prod.*, 2009, **17**(11), 1025–1029.
  - 35 D. L. Li, X. D. Jiang, Y. P. Zhang and B. Zhang, A novel route to ZnO/TiO<sub>2</sub> heterojunction composite fibers, *J. Mater. Res.*, 2013, **28**(3), 507–512.
  - 36 M. Jakob, H. Levanon and P. V. Kamat, Charge distribution between UV-irradiated TiO<sub>2</sub> and Gold nanoparticles: determination of shift in the fermi level, *Nano Lett.*, 2016, **3**(3), 353–358.
  - 37 M. G. Betti, P. Gargiani, R. Frisenda, R. Biagi, A. Cossaro, A. Verdini, L. Floreano and C. Mariani, Localized and dispersive electronic states at ordered FePc and CoPc chains on Au(110), *J. Phys. Chem. C*, 2010, **114**(49), 21638–21644.
  - 38 W. Wu, N. M. Harrison and A. J. Fisher, Electronic structure and exchange interactions in cobalt-phthalocyanine chains, *Phys. Rev. B: Condens. Matter Mater. Phys.*, 2013, **88**, 244261–244269.
  - 39 Y. H. Ao, J. Q. Bao, P. F. Wang, C. Wang and J. Hou, Bismuth oxychloride modified titanium phosphate nanoplates: a new p–n heterostructured photocatalysts with high activity for the degradation of different kinds of organic pollutants, *J. Colloid Interface Sci.*, 2016, **476**, 71–78.
  - 40 C. H. Wang, X. T. Zhang and Y. C. Liu, Promotion of multi-electron transfer for enhanced photocatalysis: a review focused on oxygen reduction reaction, *Appl. Surf. Sci.*, 2015, **358**, 28–45.
  - 41 M. Li, S. Yin, T. Wu, J. Di, M. X. Ji and B. Wang, Controlled preparation of MoS<sub>2</sub>/PbBiO<sub>2</sub>I hybrid microspheres with enhanced visible-light photocatalytic behavior, *Adv. Colloid Interface Sci.*, 2018, **517**, 278.
  - 42 L. Khachatryan, E. Vejerano, S. Lomnicki and B. Dellinger, Environmentally persistent free radicals (EPFRs). 1. Generation of reactive oxygen species in aqueous solutions, *Environ. Sci. Technol.*, 2011, **45**(19), 8559–8566.
  - 43 T. Kobayashi, The far spectra of phthalocyanine and its metal derivatives, *Spectrochim. Acta*, 1970, **26**, 1313–1322.
  - 44 J. H. Zagal, Metallophthalocyanines as catalysts in electrochemical reactions, *Coord. Chem. Rev.*, 1992, **119**, 89–136.
  - 45 T. Kroll, V. Y. Aristov, O. V. Molodtsova, Y. A. Ossipyan, D. V. Vyalikh, B. Biichner and M. Knupfer, Spin and orbital ground state of Co in cobalt phthalocyanine, *J. Phys. Chem. A*, 2009, **113**, 8917–8922.
  - 46 J. P. Graham and G. Brown, Molecular orbital studies of nitrosyl metalloporphyrin complexes, *J. Arkansas Acad. Sci.*, 2011, **55**, 31–42.
  - 47 B. M. Hoffman and M. A. Ratner, Jahn-Teller effects in metalloporphyrins and other four-fold symmetric systems, *Mol. Phys.*, 2015, **35**(4), 901–925.
  - 48 R. Othman, A. L. Dicks and Z. G. Zhu, Non precious metal catalysts for the PEM fuel cell cathode, *Int. J. Hydrogen Energy*, 2012, **37**, 357–372.
  - 49 J. H. Zagal, S. Griveau, F. Silva, T. Nyokong and F. Bedioui, Metallophthalocyanine-based molecular materials as catalysts for electrochemical reactions, *Coord. Chem. Rev.*, 2010, **254**, 2755–2791.
  - 50 Y. He, L. Zhang, B. Teng and M. H. Fan, New application of Z-scheme Ag<sub>3</sub>PO<sub>4</sub>/g-C<sub>3</sub>N<sub>4</sub> composite in converting CO<sub>2</sub> to fuel, *Environ. Sci. Technol.*, 2015, **49**(1), 649–656.

